Bull Volcanol
DOI 10.1007/s00445-009-0317-3

RESEARCH ARTICLE

Tephra dispersal and eruption dynamics of wet and dry phases of the 1875 eruption of Askja Volcano, Iceland

R. J. Carey · B. F. Houghton · T. Thordarson

Received: 8 October 2008 / Accepted: 24 August 2009

Abstract The 1875 rhyolitic eruption of Askja volcano in Iceland was a complex but well-documented silicic explosive eruption. Eyewitness chronologies, coupled with examination of very proximal exposures and historical records of distal deposit thickness, provide an unusual opportunity for study of Plinian and phreatoplinian eruption and plume dynamics. The ~17 hour-long main eruption was characterized by abrupt and reversible shifts in eruption style, e.g., from 'wet' to 'dry' eruption conditions, and transitions from fall to flow activity. The main eruption began with a 'dry' subplinian phase (B), followed by a shift to a very powerful phreatoplinian 'wet' eruptive phase (C1). A shift from sustained 'wet' activity to the formation of 'wet' pyroclastic density currents followed with the C2 pyroclastic density currents, which became dryer with time. Severe ground shaking accompanied a migration in vent position and the onset of the intense 'dry' Plinian phase (D). Each of the fall units can be modeled using the segmented exponential thinning method (Bonadonna et al. 1998), and three to five segments have been recognized on a semilog plot of thickness vs. area$^{1/2}$. The availability of very proximal and far-distal thickness data in addition to detailed observations taken during this eruption has enabled calculations of eruption parameters such as volumes, intensities and eruption column heights. This comprehensive dataset has been used here to assess the bias of volume calculations when proximal and distal data are missing, and to evaluate power-law and segmented exponential thinning methods using limited datasets.

Keywords Askja 1875 · Phreatoplinian · Plinian · Eruption dynamics · Tephra dispersal

Editorial responsibility: J. Stix

R. J. Carey (✉) · B. F. Houghton
Dept. of Geology and Geophysics, University of Hawai`i,
Honolulu, HI 96822, USA
e-mail: beccarey@hawaii.edu

T. Thordarson
School of GeoSciences, University of Edinburgh,
Edinburgh EH9 3JW, UK

Introduction

The 1875 eruption of Askja volcano, Iceland, was one of very few eruptions to include both phreatoplinian and Plinian phases, and represents the only historical 'type' example of phreatoplinian volcanism (Self and Sparks 1978). During this eruption, three abrupt shifts between subplinian, phreatoplinian, pyroclastic surge and Plinian activity occurred, representing abrupt changes in eruption style (wet vs. dry) and eruption regime (fall vs. surge). Well preserved, very proximal and far-distal fallout deposits coupled with documented historical accounts taken prior to, during, and immediately after this eruption have provided a large dataset with which to calculate the 1875 eruption parameters with accuracy and infer the vent locations active throughout the main eruption. This dataset also enables us to evaluate the influences of shifting vent positions and mass discharge rates on eruption dynamics. Studies of these deposits provide a valuable dataset from which further transport and deposition models of wet and dry eruption plumes can be developed.

Location and geological setting

Askja central volcano (locally known as Dyngjufjöll) is situated in the North Volcanic Zone (NVZ), which delineates the divergent plate boundary in north Iceland (Fig. 1). The Askja volcanic system, in which the central

Published online: 09 October 2009

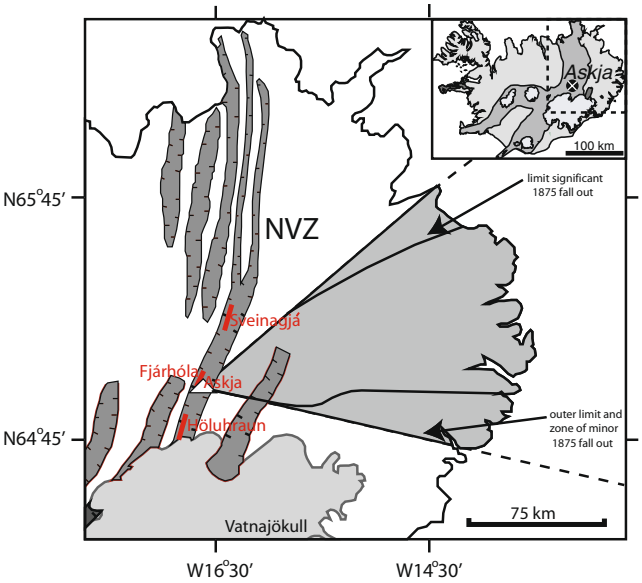

Fig. 1 Geologic setting of the Askja volcano: The Askja central volcano is located on the Askja volcanic system in the North Volcanic Zone (NVZ). Sveinagjá, Fjárhóla and Höluhraun fissures located to the north and south of the Askja volcano are sites of effusive basaltic eruptions associated with the Askja volcano-tectonic episode (1867–1876) (Thordarson et al. in prep). The dispersal areas of significant, and minor 1875 tephra fallout across east Iceland are shown

volcano sits, is 10 – 15 km wide and 100 km long. The 45 km^2 central volcano Askja rises to more than 800 m above its surroundings and contains three calderas, the second oldest of which (Askja) is 7×7 km wide and almost completely infilled with post-glacial basaltic lava (Sigvaldason 2002). The 1875 eruption, which is the subject of this paper, was responsible for the youngest caldera, which formed post-eruption in a step-wise manner for 44 years after 1875. The caldera is 3×4 km in aerial extent and today is filled by Lake Öskjuvatn (Fig. 2a). Askja volcano was largely built by basaltic sub-glacial and subaqueous activity forming hyaloclastites and to a lesser extent by interglacial and Holocene subaerial basaltic lava flows (Sigvaldason 1979; 2002). Two powerful explosive silicic eruptions are known from Askja in Holocene times, the 1875 eruption and an older event, which is not well constrained volumetrically or temporally. Throughout postglacial times, activity at Askja has been vigorous with a number of basaltic eruptions on ring fractures surrounding the caldera rim, as well as flank eruptions (Thordarson et al. in prep.). The most recent activity appears to be controlled by lithospheric extension producing an en echelon array of north-northeast to south-southwest fissures that cut the main caldera ring fractures (Brandsdottir 1992).

The 1875 eruption and subsequent caldera formation occurred during a rifting episode along the entire volcanic system. Early precursory activity at Askja prior to the 28th – 29th March phase includes eruptions that produced two basaltic phreatomagmatic tuff cones, two silicic lavas and a dike, and an obsidian-bearing small pyroclastic cone (Thordarson et al. in prep). Other eruptive activity (excluding the main phase) included extrusion of basaltic lava further out on the fissure swarm, most notably at Sveinagjá and Fjárhólahraun, 40 and 5 km north of Askja, and Holuhraun situated ~15 km south of the caldera (Fig. 1: Sigurdsson and Sparks 1978a, Sigurdsson and Sparks, 1978b; Brandsdottir 1992; Sigurdsson 1978a, b). Phreatic and basaltic phreatomagmatic activity continued after the main eruption well into 1876 (Sigvaldason 1979; Sparks et al. 1981; Thordarson, unpublished data). Post-1876 activity included both explosive and extrusive eruptions of basaltic magma in 1921–22, 1929, 1931 and 1961 (Sigvaldason 1979; Sparks et al. 1981). All the pyroclastic vents that were active during the March 28th – 29th, 1875 eruption sequence are located within the present day Lake Öskjuvatn.

28th – 29th March 1875 eruptive sequence

The pyroclastic deposits of the Askja 1874–75 eruption were divided into six units (A – F) by Self and Sparks (1978) and Sparks et al. (1981). In this scheme, the formation of units A, E and F are correlated with weak phreatic or hydrothermal activity prior to and following the main phases (units B, C1, C2 and D). Magmatic eruptive activity of the main eruption, beginning on 28th March, had four distinct intervals of different intensity and style (Fig. 2b). The eruption began with a subplinian phase (forming unit B), followed by a phreatoplinian fall phase (unit C1). Dilute density currents (unit C2) were emplaced after the phreatoplinian fall but were largely confined to the larger Askja caldera region. The final phase was a Plinian eruption (unit D). In detail, the Plinian deposits in the proximal area can be separated into five distinct sub-units with contrasting dispersal, grain size and componentry (Fig. 2b). D1, D3 and D5 are widely dispersed sub-units and cannot be separated outside of the caldera, where they merge, forming medial-distal unit D with thinning half ($t_{½}$) distances of 3 – 4 km. D2 and D4 thin and fine more rapidly, with radial thinning half distances 1 to 2 orders of magnitude less (10 s to 100 s of meters), and are the products of fountaining from separate vents that were synchronous with Plinian activity (Carey et al. 2008a).

28th – 29th March 1875 deposits

The 1875 deposits are well exposed along the caldera rim and particularly towards the east along the dispersal axis (Fig. 2a). At the time of the eruption, thick snow cover was present in the proximal and medial areas (Thoroddsen 1913; Thordarson et al., in prep). The 1875 deposits accumulated on this snow and were subject to local

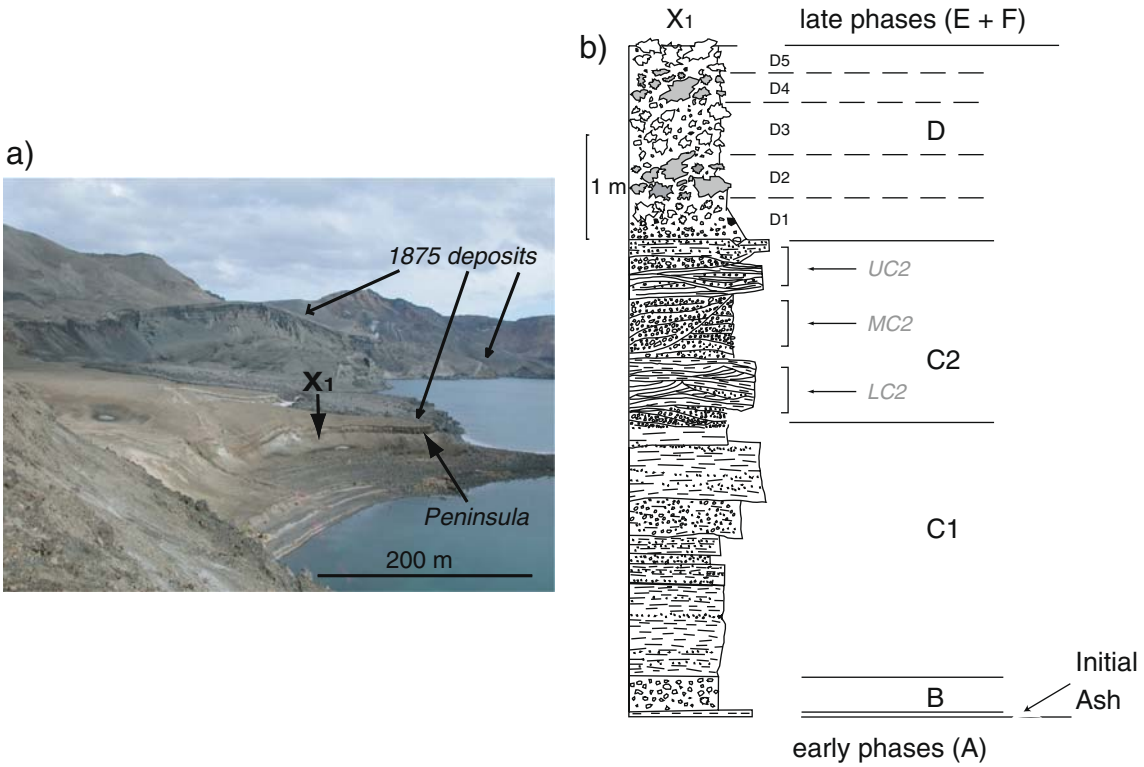

Fig. 2 Photograph of the northeastern side of the caldera, view to east along the dispersal axis. Note in the foreground the alternating white-grey stratigraphy of sub-units within unit D on the peninsula. White C2 pyroclastic surge and C1 phreatoplinian ash lie underneath. The ash mantles the faulted and downthrust blocks to the left, which have dropped due to caldera collapse after the 1875 eruption. The stratigraphy at X_1 is shown (right), the nomenclature has been adapted from Self and Sparks (1978) and Sparks et al. (1981). The C2 pyroclastic surge deposits have been split into three flow units (lower, middle and upper), and the Plinian unit D deposits are subdivided into five separate sub-units as defined in Carey et al. (2008a)

reworking. The annual thick snowfall and seasonal melting in the highlands surrounding Askja subsequently led to high degrees of erosion and reworking in the proximal environments especially on the volcano. In addition, there is also some evidence for syn-eruptive mass failure and slumping of C1 and C2 tephra in the most proximal exposures. However, true primary thicknesses are locally well preserved in many places, especially in topographic lows. This is particular true for units B and C which were protected by Plinian fall D, and these exposures provide very good control on proximal stratigraphy. In the medial to distal areas, historical records highlight the very bad weather conditions two days after the eruption, and the deposits were eroded and reworked significantly. Tephra was eroded from topographic highs and deposited in lows, which necessitates very careful interpretation of even contemporary medial/distal thickness data.

Initial Ash (Fall)

A white, very fine-grained ash underlies the proximal subplinian deposit; it is patchily distributed in the medial area.

Unit B (Fall)

The first widespread magmatic unit of the 28th – 29th March eruption sequence is a subplinian fall deposit which is reversely graded, well sorted and has a maximum thickness of 56 cm at the most proximal site situated about 950 m downwind from the inferred source vent. The pumices typically range from fine to coarse lapilli with rare bombs up to 15 cm in diameter (Fig. 3a). Lithic clast abundance in the unit B deposit ranges from 5 – 25 modal wt.% and decreases systematically with distance from vent. The lithic clasts are predominantly non-to-poorly vesicular obsidian fragments (80 modal wt.%); grey basaltic lava fragments and red-oxidized hyaloclastite are minor components. The Unit B pumice fall has a narrow east-directed dispersal and forms a tephra sheet extending out to ~50 km from the source. It did not reach inhabited areas in east Iceland. This unit is capped by the very fine phreatoplinian ashfall deposit, unit C1 (see below), which infiltrates the interstices of the coarse B pumice fall deposit in all areas.

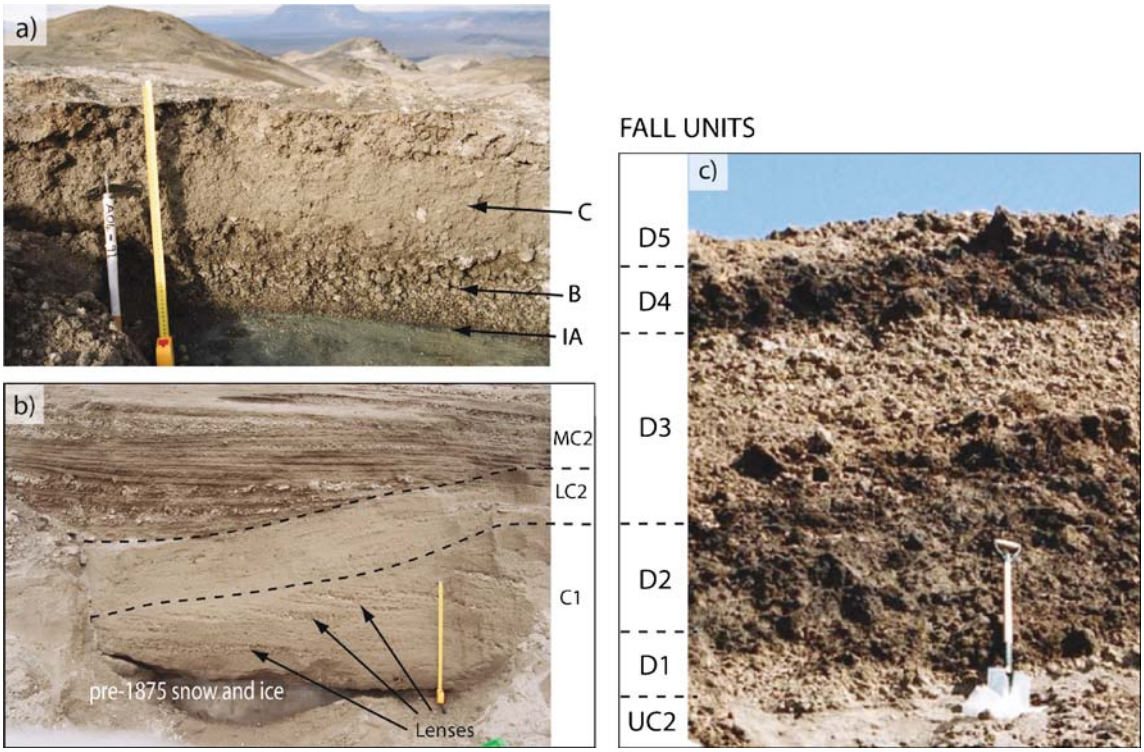

Fig. 3 Photographs of the 1875 pyroclastic units. **a** unit B in a medial location. It has a salt and pepper texture due to the abundance of obsidian and basaltic lava fragments in addition to minor grey micro-vesicular clasts (Tool is 32 cm for scale). Partial thicknesses of unit C lie above unit B, however unit D is removed. **b** Unit C in a proximal caldera outcrop. The C1 phreatoplinian fall unit is at the base and contains discrete lenses of fine lapilli. There are two major erosional unconformities visible in this outcrop as indicated by dashed lines. The lower is the erosion of C1 due to the erosive lower C2 surge currents. The upper is the erosion of lower C2 deposits by middle C2 surge currents. Tape measure is 80 cm for scale. **c** The unit D deposits at a proximal section X_1 on Figure 2. This photograph shows all five sub-units of D. D2 and D4 are related to a separate series of vents that were erupting in weaker fountaining fashion (Carey et al. 2008a, b). The grain size of the D1, D3, D5 deposits becomes coarser with time, so that D5 comprise the coarsest ejecta

Unit C1 (Fall)

Unit C1 is a phreatoplinian fall deposit consisting of very fine, pale grey, uniformly massive ash (Fig. 3b). In the medial-distal area, it is inferred that a component of C2 co-surge ash overlies C1, and collectively the deposit is simply referred to as unit C. Proximal unit C1 has a maximum thickness of 228 cm along the southeast sector of the Öskjuvatn caldera. Similar meter-scale thicknesses are maintained at proximal sites to the north, east and west of the caldera. In the most proximal sites within three kilometers of the vent, C1 contains sporadic lenses of sub-angular to sub-rounded pumice lapilli as well as single-grain-thick trains of lapilli-sized pumices. Grain size analyses conducted by Sparks et al. (1981) suggest that 99 wt.% of this deposit is finer than 1 mm. In many of the medial and distal locations, the C ash is vesiculated with mm-sized cavities, but accretionary lapilli are rare. Lithics within this unit occur predominantly in the ash-size fraction; however, rare >1 cm diameter lithic clasts are also present in the deposit at the most proximal sites. The lithic population has a modal abundance of<5 wt.% and consists predominantly of obsidian shards together with minor amounts of basaltic lava fragments. Unit C is widely dispersed to the east-northeast, extending over eastern Iceland and Scandinavia (Sparks et al. 1981). The most distal sites within Iceland, at ~150 km from source, have a thickness of 5 mm whereas in Scandinavia, 1200 to 1500 km distant, very fine sub-millimeter ash fall was reported (Mohn 1878). In the proximal area, unit C1 is overlain by C2 density current deposits (Figs. 3b, 4a, b). Outside the caldera, clasts from Plinian fall unit D impact into and sit upon unit C.

Unit C2 (pyroclastic surge)

Following the C1 phreatoplinian fall deposits, three major intervals of pyroclastic surge deposition occurred; these have been named lower, middle and upper C2 (Fig. 4). These three phases varied in intensity and degree of water involvement with time. The first dilute density current deposits (LC2) are extremely ash-rich, with poorly-sorted fine to medium lapilli lenses, lacking well-sorted fine to coarse pumice lenses, and commonly heavily erode C1 in

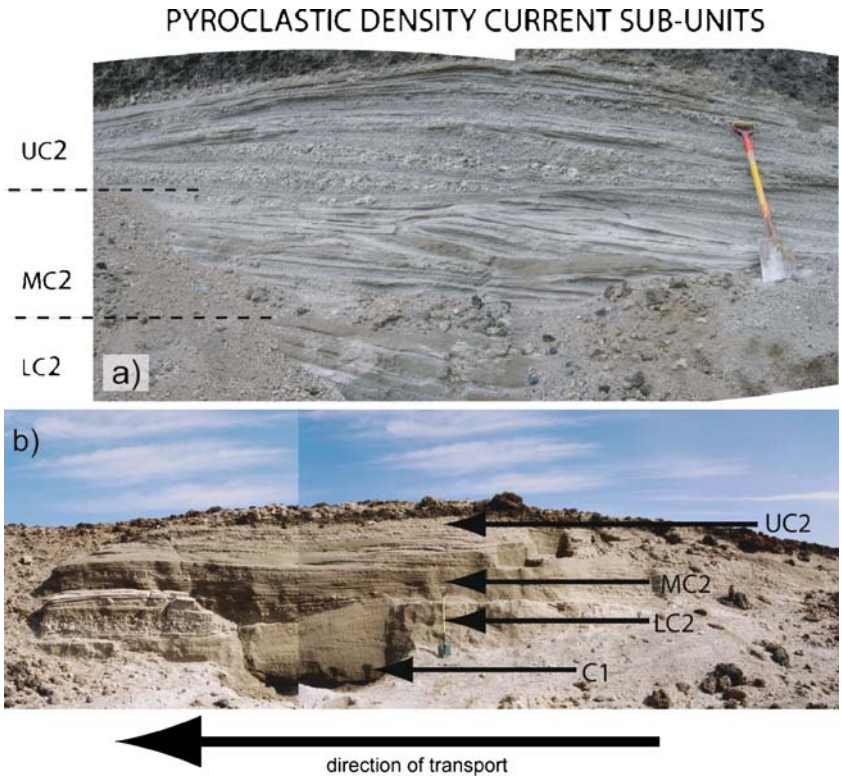

Fig. 4 Photographs of outcrops on the Öskjuvatn caldera margin, exemplifying the current bedforms of the C2 pyroclastic surge deposits. **a** Lower C2, Middle C2, Upper C2 deposits. See text for details. All C2 flow units exhibit similar directions of transport towards the left of picture. Unit D is above. Shovel is 1 meter for scale

the proximal area. The MC2 dilute density current deposits are also ash-rich. However, well-sorted fine to coarse pumice lenses are common, and these currents often eroded LC2 and C1 deposits (Figs. 3b, 4a, b). The upper C2 (UC2) deposits have well-defined bedsets, a higher abundance of well-sorted pumice lenses which are fines-poor, and contain rounded coarse lapilli. The UC2 bedforms have longer wavelengths, higher amplitudes and also erode underlying deposits (Fig. 4). Bedform directionality of all C2 deposits points to radial transport from a vent now situated within the north-central part of Öskjuvatn. All of the dilute density current deposits were largely confined within the older caldera, with minimal runout over the lower topography in the southwest portion of the older caldera walls.

Unit D (Fall)

The Plinian fall deposits are the final erupted products of the main eruption (Fig. 3c). In the proximal area, the widespread Plinian D1, D3 and D5 sub-units define a trend of reverse grading with an increasing median grain size of −3.2, −5.3 and −6.1 phi respectively at our type locality (Carey et al. 2008a). Inman (1952) sorting values (σ_ϕ) of these sub-units range from 1.6 to 2.5 (Carey et al. 2008a). In the medial area, the D1, D3 and D5 sub-units are amalgamated into a single inverse-graded, moderately-sorted fall unit (0.6 – 1.4; Inman 1952). A weak two-fold subdivision in the medial/distal areas is superimposed on the overall trend of reverse grading, and identified based on lithic abundance. The lowermost part contains approximately 5 – 10 modal wt.% lithic clasts that are dominantly obsidian and basaltic lava fragments. The upper part is comparatively lithic-poor, with lithic abundances<5 modal wt.%, comprising dominantly obsidian with minor basaltic lava fragments and rare granophyre.

Distal deposits of Plinian fall up to 150 km from vent are moderately well sorted (0.15 – 1.1; Inman 1952) and are up to 2.0 cm thick at the most distal Icelandic location along the dispersal axis. In Scandinavia, 1100–1500 km from Askja, reported thicknesses of freshly fallen ash range from 0.3 mm to 3 mm (Nordenskiöld, 1876). However, we are unable to discriminate between the relative contributions to this deposit from units C and D from the historical reports.

Distribution and thickness of the depositional units

All fall units erupted during the main eruption over a ~17 h period on 28th – 29th March 1875 were dispersed to the east, although each had slightly different dispersal direction. The dispersal of the subplinian fall B is to the northeast, but its deposition is entirely confined to the highlands above the rural communities in eastern Iceland. The fall deposits of the phreatoplinian and Plinian phases (C and D) are more widely dispersed, and information from contemporary reports and interviews was used by Mohn (1878) to draw an isochron

map of the Askja 1875 plume dispersal as it traveled from Askja and over Scandinavia. This isochron map, in addition to quantitative thickness and isomass measurements of tephra fall at sites in Scandinavia (Nordenskiöld 1876) and analysis of the prevailing wind pattern during that season, has allowed us to constrain the isopachs of both phases in the far-distal field (Mohn 1878). The isopach maps presented here are constructed using four sets of data:

1. Deposit logs, measurements of deposit thickness and maximum clast size at 488 new sites across eastern Iceland, including documenting sites of zero thickness. Care was taken to measure primary thicknesses in multiple pits at one location and preferably in topographic lows, where deposits represented primary thicknesses.
2. New bulk deposit density measurements for the tephra of units C and D along the dispersal axis.
3. Collation of reported 'in situ' thickness measurements of the March 29th 1875 deposit in eastern Iceland made at the time of the eruption (Phases C and D) (Mohn, 1878; Thordarson et al. in prep). Our own observations and thickness measurements of the deposits at the same sites allow us to calculate compaction factors.
4. Collection and analysis of reliable observations, including deposit thickness and particularly mass per unit area data, of the March 28th – 29th 1875 deposits obtained from contemporary descriptions in Norway and Sweden compiled by Nordenskiöld (1876) and Mohn (1878) immediately after the eruption.

Integrating the historical and modern thickness data

First, at the 488 new localities that were visited in 2004–2006, we have logged and described the Askja March 28th – 29th deposit and measured unit thicknesses. Second, the distal measurements of thickness made in Scandinavia at the time of the eruption have been adjusted from the measured uncompacted thickness to compacted values using a compaction ratio of 0.5. This compaction ratio is obtained by comparing thickness measurements of units C and D taken shortly after the eruption in the medial and distal fields in Iceland and reported in the historical accounts, with our own thickness measurements at the same locations in 2005 – 2006. Some issues arose with the historical Scandinavian data because it was difficult to interpret whether deposit thickness had been measured by the observers in areas of syn-and post-eruptive reworking. Many reported measurements are clearly overthickened. For this reason, we have given emphasis to three isomass measurements made where tephra was collected over extended and undisturbed measured areas. Our third approach to integrate thickness data was to use historical accounts where thin ashfall was observed, but could not be measured, to establish a "visual trace isopach". The visual trace isopach has been assigned an equivalent mass per unit area (2 $g m^{-2}$), and equivalent thickness value of 10^{-3} mm, based on the recorded outer limit for four historical Plinian and subplinian eruptions, particularly the visual trace we measured for the 17 June 1996 eruption of Ruapehu volcano, New Zealand (Bonadonna and Houghton 2005). Finally, the presence or absence of known 1875 ash shards in peat bogs through Norway, Sweden, Germany and the Faeroe Islands define a "detected limit" isopach. The detected limit represents an outer limit to the 1875 ash fall. We have assigned an equivalent (or pseudo) thickness value of 10^{-4} mm, which was converted from mass per unit area in the peat deposits, which in turn is obtained from calculations of number of ash particles (20 – 40 microns in size) identified within a known volume of peat, as documented in northern Germany, Sweden, and Norway (Persson 1971; Oldfield et al. 1997; van den Bogaard et al. 2002; Boygle 2004; Pilcher et al. 2005).

The historical reports and distal thickness measurements in Scandinavia do not discriminate between the products of the phreatoplinian and Plinian plumes, hence it is impossible to constrain robustly the individual thicknesses of C and D tephras. At the most distal point in Iceland, where thickness measurements of C and D tephra were collected, the thickness ratio of unit C to unit D ash was approximately 1:3. This ratio is our best estimate of the relative contribution of the two units, and has been adopted in partitioning the ash fall in the far-distal fields in Scandinavia.

Subplinian unit B

The subplinian fall began at 9 PM (local time) on the 28th March 1875, when "a pitch black column of smoke was seen rising from Askja and was visible for only one hour due to the approaching darkness" (Thoroddsen 1913). The proximal to distal isopachs of the subplinian fall of unit B, as shown on Fig. 5a, define a narrow dispersal to the east-northeast which is extremely attenuated in the proximal to medial areas, as defined by the 50 – 5 cm isopachs. Isopachs of 2 and 3 cm thickness extend up to 34 km downwind from vent and are also extremely narrow. The 2, 1 and 0.5 cm isopachs in the distal area spread increasingly wider, both crosswind and downwind, and the latter shows the greatest crosswind expansion (Fig. 5a).

Phreatoplinian unit C

Analysis of historical accounts indicates the onset of the phreatoplinian C1 eruption was around 5:30 AM (local time) on the 29th March and lasted for approximately 1 h (Thordarson et al. in prep). According to the historical accounts the dispersal of the phreatoplinian plume was to the east-northeast by strong winds (~ 20 $m s^{-1}$) in the upper atmosphere and involved fallout of a "wet, sticky gray ash"

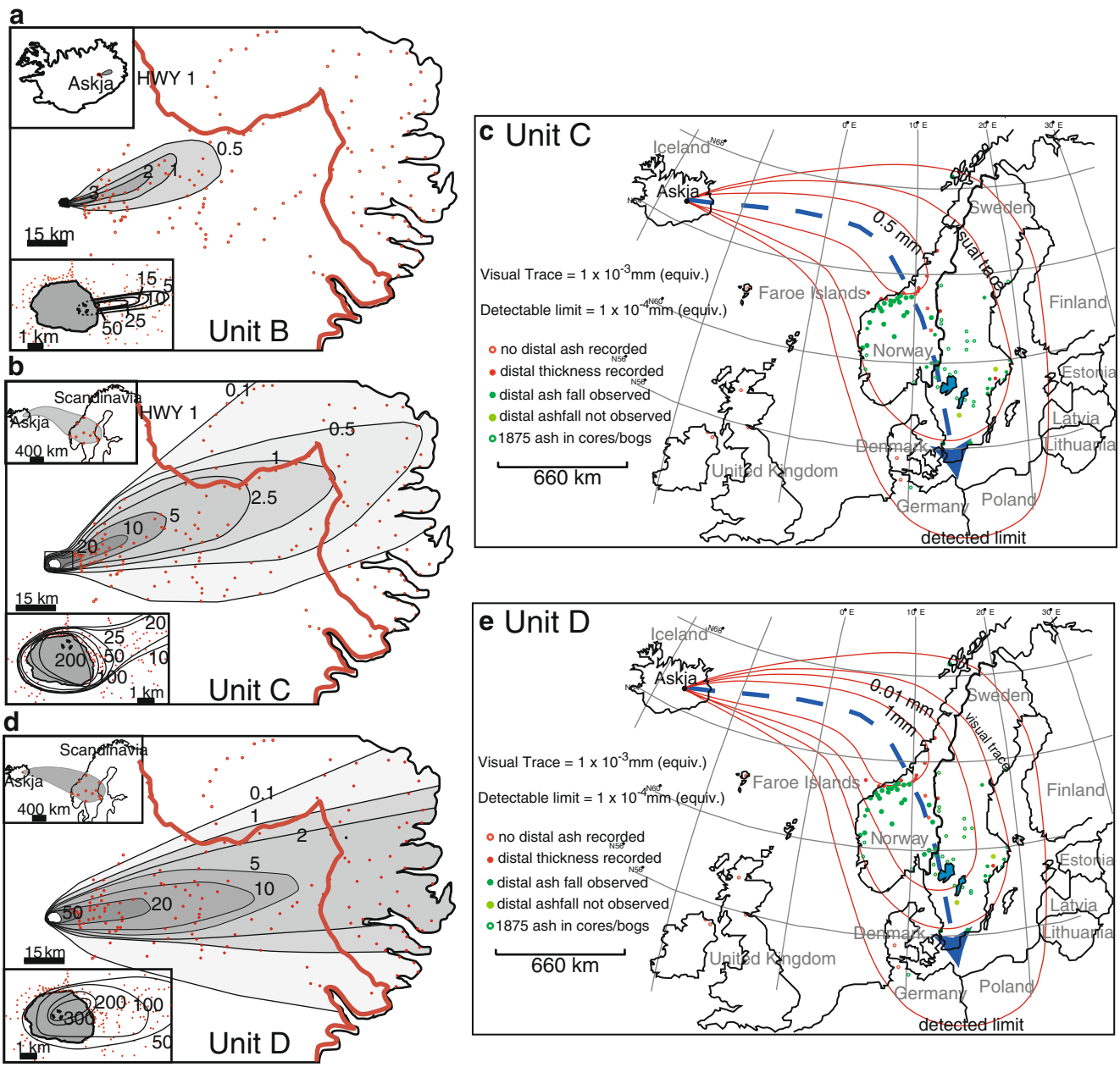

Fig. 5 Isopach maps of the units B, C, and D fall deposits. Isopachs are given in centimeters. **a** The unit B deposits are elongated and distributed towards the east in the proximal/medial area. However, more distally unit B has been distributed towards the north east. **b** The unit C isopachs in the proximal environment are circular, but become elongated when the deposit is <20 cm in thickness. The isopachs show a northeastern dispersal. Unit C has a thickness of 0.5 cm on the east coast of Iceland. **c** Far-distal isopach map of unit C. The deflection described by Mohn (1877) fits with data from inhabitants within the dispersal area. **d** Isopach map for unit D. The proximal isopachs are elongated toward the northeast/east. **e** The far-distal isopachs of unit D

in medial to distal areas (e.g., Thoroddsen 1913). Preserved thicknesses of ash from this phase are most likely to be primary, due to its wet adhesive nature and the fact that it was almost immediately covered by the unit D Plinian pumice fall. The proximal, medial and distal isopachs of the phreatoplinian phase have distinctly different geometries (Fig. 5b). In the proximal area, the 200, 100, 50 and 25 cm isopachs have near-circular to ellipsoidal shapes (Fig. 5b). The 20 and 10 cm isopachs are attenuated toward the northeast, and on a cross-axis transect at approximately 12 km from source; the 5, 2.5, 1 and 0.5 cm isopachs show drastic radial expansion, whereas the 20 and 10 cm isopachs are narrower. The 0.1 cm isopach is extremely attenuated towards the northeast and east. The far-distal

isopachs curve southward over Scandinavia, indicating a sharp deflection to the south as the plume traveled over the landmass, which is typical of the wind fields during late winter in this northern region (Fig. 5c).

Plinian unit D

After approximately a 30 min pause in tephra fall in eastern Iceland, reports from mid-eastern Iceland (Jokuldalur, 62 km east of Askja) indicate a renewed phase of pumice fall (Thoroddsen 1913). A summary of the historical reports indicate that ash fall began and stopped significantly later at localities farther to the south, suggesting a southward shift of the main dispersal axis with time (Thoroddsen 1913). The medial to distal isopachs of the Plinian phase are much wider in a cross-transport direction than those of other eruptions at similar distances (e.g., Mount St Helens; Sarna-Wojcicki et al. 1981; Chaiten 2008; see reference in Watt et al. 2009), which may be explained by such a southward migration of the wind direction during the D phase (Fig. 5d). In the proximal region, the 300, 200, 100 and 50 cm contours are all strongly ellipsoidal to the east of the Öskjuvatn caldera (Fig. 5d). In the medial and distal areas, the 20, 10, 5, 2 and 1 cm isopachs are also strongly ellipsoidal towards the east, but show crosswind expansion. In the very distal area the isopachs trend eastwards before turning south over Scandinavia and extending as far as northern Germany (Fig. 5e). Peat bogs in the Faeroe Islands, British Isles and Scotland show no signs of 1875 tephra and constrain the detected limit isopach (Fig. 5e) (Persson 1971; Oldfield et al. 1997; van den Bogaard et al. 2002; Boygle 2004; Pilcher et al. 2005).

Clast size distribution

The maximum sizes of pumice and lithic clasts within each unit of the 1875 deposits were documented at each location by measuring and averaging the three principal axes of five largest clasts.

Subplinian unit B

In the proximal area, pumice clasts to 100 mm and lithics of 20 mm diameter are found up to 1 km from the inferred vent. The 100, 75 and 50 mm proximal pumice isopleths are very elongate with narrow cross- and upwind extents (Fig. 6a). A similar but even narrower trend is observed for the 10 mm lithic isopleth (Fig. 6b). The medial to distal pumice isopleths (20, 10, 5 mm) are much more expanded than their proximal counterparts. The medial lithic isopachs, however, do not exhibit this expansion until approximately 4 km from vent, as shown by the 10 mm isopleth. In terms of dispersal, the lithic isopleths show a migration from an eastward axis (10 mm) to a northeasterly direction (7.5, 5, 2.5 mm), which is not observed in the pumice isopleths (Fig. 6a, b).

Phreatoplinian unit C

Pumice isopleths (70 and 50 mm) in the proximal and medial areas are narrowly ellipsoidal, only expanding more significantly crosswind at approximately 9 km downwind from the inferred vent (Fig. 6c). The proximal lithic isopleths (>10 mm) mirror those of the pumice. However, they are more strongly ellipsoidal with the exception of the most proximal isopleth (70 mm) which is circular (Fig. 6d). Medial pumice isopleths (20 and 10 mm) show a crosswind expansion and northward migration which is mirrored in the lithic isopleths (7.5, 5, 2.5 mm). Distal pumice (5, 2.5 mm) and lithic isopleths (1 mm) are expanded greatly crosswind and show a more northward trend than those of the proximal-medial isopleths. These trends together with the isopach data suggest a westerly wind direction for lower elevations which then becomes more southerly with increasing plume height.

Plinian unit D

The isopleth maps show complex geometries throughout the proximal to distal areas. In the proximal area, the lithic and pumice isopleths are initially circular but become ellipsoidal with increasing distance from vent (Figs. 6e, f). The 500 mm pumice isopleth and 50 mm lithic isopleth reflect a northeastern dispersal direction that changes to more eastward for smaller isopleths. With the exceptions of the 50 mm pumice isopleth and 5 mm lithic isopleth, the medial to distal isopleths follow a eastward to slight northward dispersal direction, with greater crosswind expansion with increasing distance from vent (Figs. 6e, f). In comparison to the earlier phases of this eruption, the pumice and lithic isopleths in proximal to distal areas are wider crosswind, and less ellipsoidal, and there is more expansion in the isopleths closer to vent. The southward migration of the wind during the period of Plinian tephra fall probably accounts for the expanded medial/distal isopleths in comparison to other phases.

Eruptive parameters

Volume calculations

Volume of a tephra fall deposit is the key parameter in terms of establishing the magnitude and intensity of an eruption. Calculations of volume for medium to large scale eruptions are generally difficult for preservation reasons,

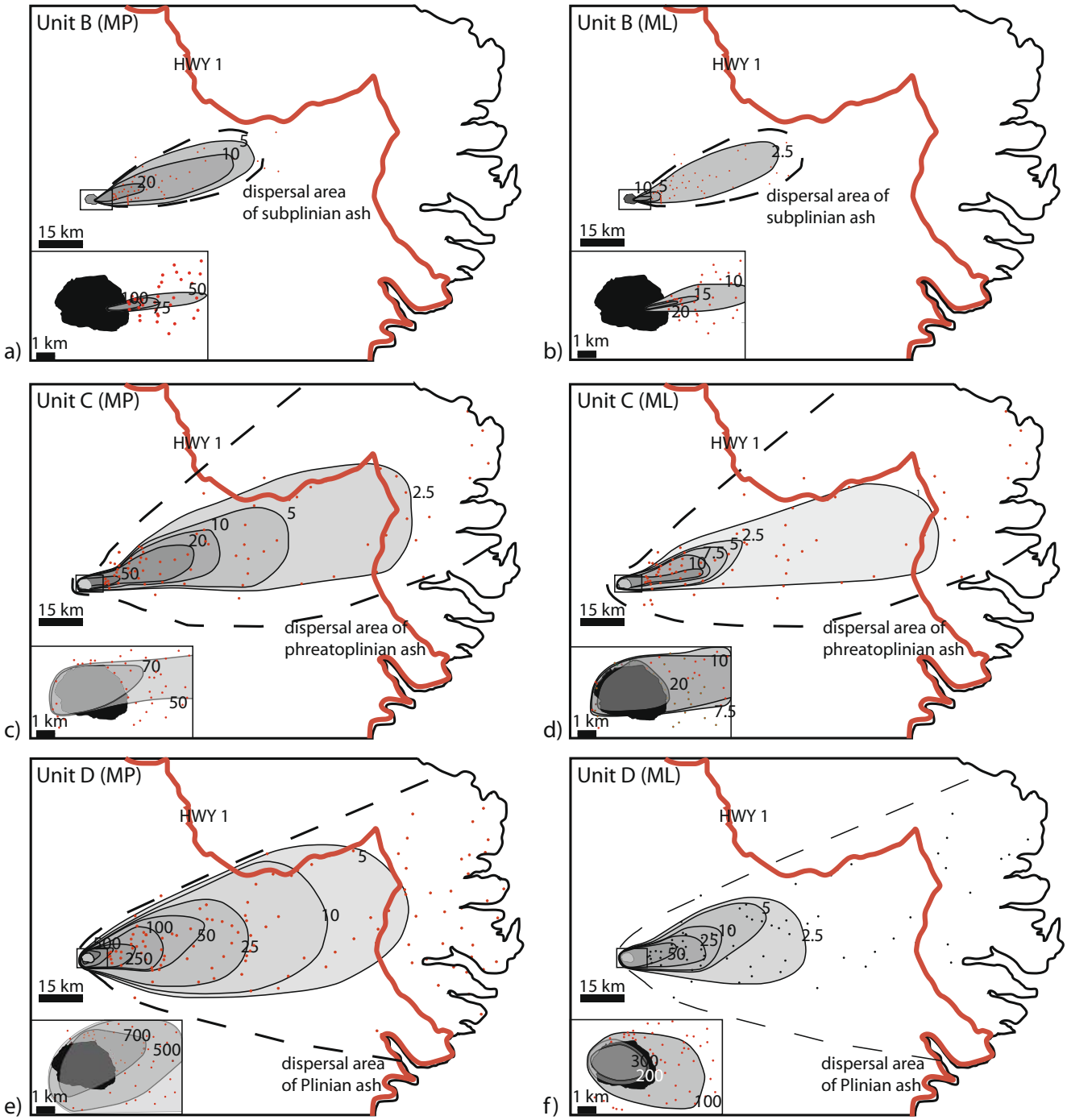

Fig. 6 Isopleth maps of units B, C, and D. Measurements are given in millimeters. The outlines of the dispersal areas are shown. The x, y, and z axes of the five largest pumices and lithics at every site were measured. **a** and **b** maps showing the maximum pumice (MP) and maximum lithic (ML) isopleths for unit B. **c** and **d** unit C isopleth maps showing the dispersal of the largest pumice and lithic clasts. **e** and **f** isopleth maps of the unit D deposits. Note the angularity of the southern arm of the 50 mm MP and 5 mm ML isopleths. These observations together with field work suggest that severe erosion has taken place in this sector

for example due to the absence of thickness data in the proximal region, e.g.,~< 4 km from vent for Taupo 181 AD (Smith and Houghton 1995a, b) and/or in the distal field, e.g., due to tephra dispersal over the ocean (e.g., Quizapu 1932, see reference in Hildreth and Drake 1992; Hudson 1991, see reference in Scasso et al. 1994). The 1875 eruption is unique in that proximal exposures up to 1 km from vent are accessible while far-distal thickness data are available for equivalent-thickness values of 10^{-2} to 10^{-5} cm. The dispersal of tephra in Iceland has well-constrained

proximal to near-distal isopachs for each phase (< 150 km east of vent), and data from sites in Scandinavia and Germany uniquely constrain the far-distal field of tephra dispersal (1100 km to 2000 km from source). Thus, this eruption permits the relationship between thickness and dispersal area to be accurately quantified. Each of the fall units have been plotted on a semi-log plot of thickness vs. area$^{1/2}$, after Pyle (1989), to identify thinning trends (Fig. 7). We use both exponential thinning and power-law methods to compare and contrast volume calculations of each fall unit of the 1875 eruption.

Exponential thinning

Numerous studies of thickness vs. area$^{1/2}$ relationships for medium to large scale eruptions show that the volume of a fall unit cannot be approximated by simple exponential thinning. The thinning relationship is better approximated by two or more segments on a plot of

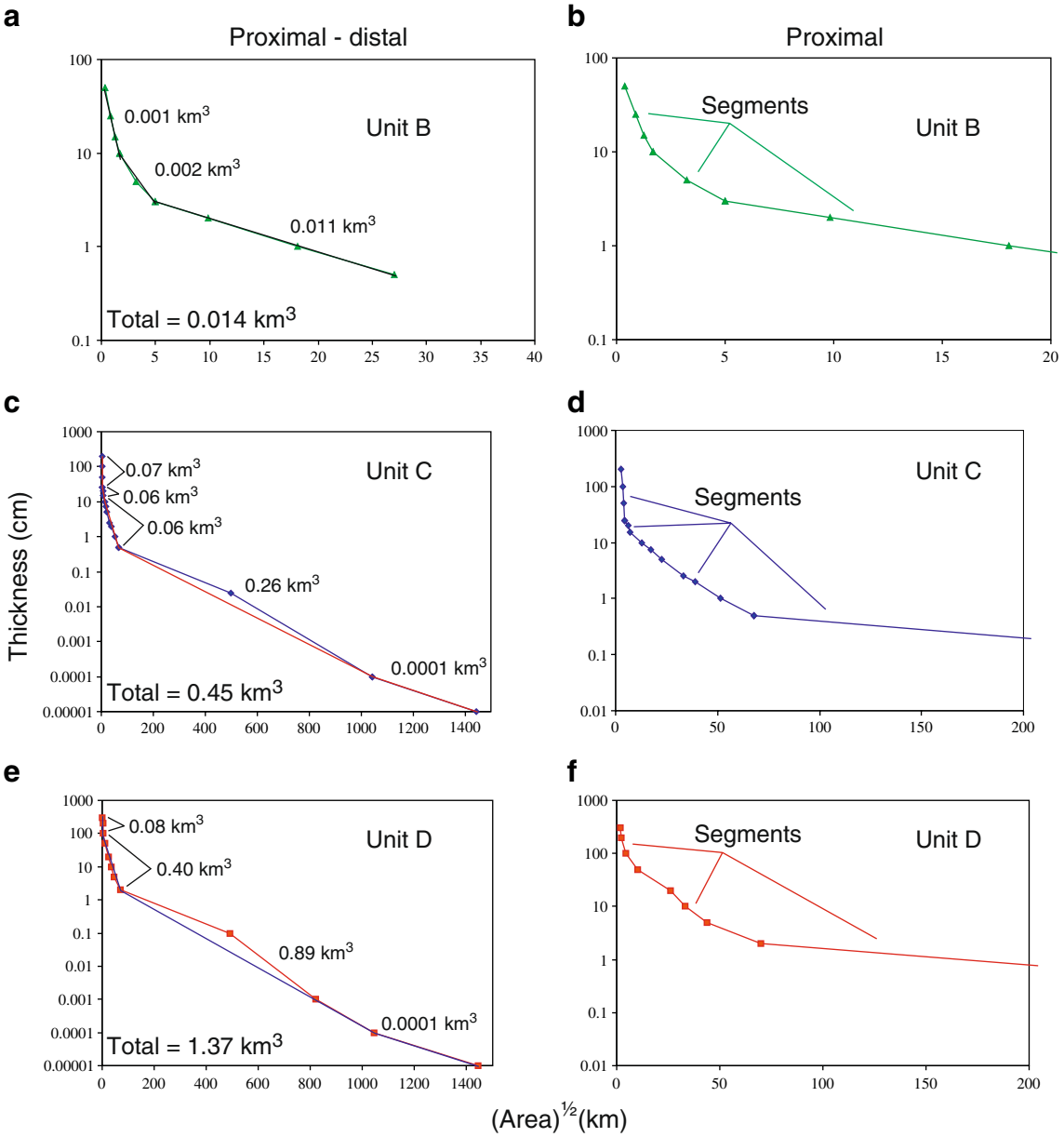

Fig. 7 Semilog plots of thickness vs. area$^{1/2}$ within the isopach for the 1875 fall units. The volumes of each segment are shown next to figures **a**, **c** and **e**. The segments are also indicated in figures **b**, **d** and **f** which show expanded views of the more proximal areas of each graph. **a** and **b**: Unit B can be approximated with three segments. **c** and **d**: Unit C can be separated into five segments. **e** and **f**: Unit D can be approximated by four segments. Note the steeply sloping, most proximal segment and the segmented nature of each fall unit

semi-log thickness vs. area$^{1/2}$ (e.g., Quizapu 1932, see reference in Hildreth and Drake 1992). Fierstein and Nathenson (1992) and Pyle (1990) derived equations to calculate volumes based on two exponentially thinning segments with one inflection point. Where more than two segments can be defined, a more general formula was proposed by Bonadonna and Houghton (2005):

$$V = \frac{2T1_0}{k_1^2} + 2T1_0\left[\frac{k_2BS_1+1}{k_2^2} - \frac{k_1BS_1+1}{k_1^2}\right]\exp^{(-k_1BS_1)} + 2T2_0\left[\frac{k_3BS_2+1}{k_3^2} - \frac{k_2BS_2+1}{k_2^2}\right]\exp^{(-k_2BS_2)} + 2T(n-1_0)\left[\frac{k_nBS_{(n-1)}+1}{k_n^2} - \frac{k_{(n-1)}BS_{(n-1)}+1}{k_{(n-1)}^2}\right]\exp^{(-k_{(n-1)}BS_{(n-1)})} \quad (1)$$

Where T_{no}, $-k_n$ and BS_n are the intercept, slope, and location of the break in slope of the line segment n. The *n* values (number of segments) for the Askja deposits are 3 (subplinian), 4 (Plinian) and 5 (phreatoplinian). Given that the 1875 fall units are best approximated by three to five exponential line segments (Fig. 7), we have used the method of Bonadonna and Houghton (2005) to calculate volumes for each of the fall deposits. The number of segments, their respective volumes and breaks in slope for each fall unit are listed in Tables 1a and 2b.

Power-law thinning

Several deposits (e.g., Ruapehu, 17 June 1996) show a good fit to a power-law thinning relationship (Bonadonna and Houghton 2005). The power-law relationship is also theorized to be more applicable than exponential thinning when there is significant fine ash in the plume, as exponential thinning tends to underestimate the volumes of such deposits (Bonadonna et al. 1998; Bonadonna and Houghton 2005). The proximal and distal data appear more suited to the segmented exponential thinning model; however, we have also used the power law method described in Bonadonna and Houghton (2005), with *B* and *C* integration values (distance of calculated maximum thickness and downward limit of significant umbrella cloud spreading respectively) calculated separately for each 1875 fall unit to obtain volumes (Fig. 8; Tables 1a, 2b).

Uncertainties in far-distal 'isopachs'

The far distal isopachs (10^{-2} to 10^{-3} cm) extending outside of Iceland are moderately well constrained on the Scandinavian landmass; however, no sediment core data from the Atlantic Ocean are able to constrain the isopachs extending over the ocean. To estimate the effects of uncertainties in the distal data, we have also modeled the thinning behavior and volume assuming a 10% error in the area of each isopach. In addition, we considered the possibility of an order of magnitude increase in the thickness equivalent virtual trace and detected limit isopachs. The model results show for all these cases that the volume does not change by more than ~20%.

Vent position

Vent locations for each phase of the eruption are located within the present-day lake. However, using descriptions and drawings made weeks to months after the main eruption, knowledge of the structural fabric of the caldera region, dispersal data and deposit characteristics, we are able to infer fairly accurately where vents were located. Historical records written in February, 1875, prior to the main eruption (Thoroddsen, 1913, Thoroddsen 1925) document precursory activity occurring in the east and southeastern margin of the older caldera. In addition, a small pond had formed in a depression in the north-central part of the present-

Table 1 (a) Total volume estimates for the Askja 1875 fall units calculated using the segmented exponential and power-law thinning models. The data in each case were best approximated by the exponential thinning model, except in the case of unit B, where a power-law fit to the data gave the identical volume

Volume (km^3)

unit	first segment	second segment	third segment	fourth segment	fifth segment	exponential total	power law total	Integration limits		R^2
								B (km)	C (km)	
unit B	0	0	0.01	—	—	**0.01**	**0.01**	0	45	0.99
unit C	0.07	0.12	0.1	0.27	0	**0.45**	**0.47**	0.03	1300	0.95
unit D	0.08	0.4	0.9	0	—	**1.37**	**2.33**	0.03	1300	0.88

Table 2 (b) Break in slope (Bs) distances from vent between segments (i.e., 1 – 2 etc.) are listed for each of the 1875 fall units. Integration limits for C were chosen based on confidence in distal measurements, in addition to a distance where >95% of the total volume is already deposited

Unit	Bs (km) 1–2	Bs (km) 2–3	Bs (km) 3–4	Bs (km) 4–5
Unit B	0.9	2.4	——	——
Unit C	2.5	4.2	31	633
Unit D	2.8	27	591	——

day lake, fed by groundwater. Observations made after the main eruption document a small triangular depression, with three fracture swarms which extended from the centre of the depression: one to the southeast, one to north and one to the west-northwest (Fig. 9; Watts 1876; Jöhnstrup 1876, 1877). The present day caldera developed in step-wise fashion over 40– 45 years after the eruption. The subplinian deposits contain basaltic lava and hyaloclastite wall-rock fragments, and the narrow crosswind widths of the isopach and isopleth data suggest that this vent was located near the easternmost side of the present day lake, i.e., at the contact of the hyaloclastite walls of the Askja caldera and the caldera-filling basaltic lavas (Fig. 9). This location lies within the NW-SE trending fault swarm and is the easternmost vent position throughout the eruption.

The isopachs and isopleths for the phreatoplinian C phase are difficult to interpret in terms of a precise vent location due to the location of the present-day lake and the circular nature of the proximal isopachs. Due to the wet nature of the C2 density currents, we infer that they were erupted from a geographically similar location to the phreatoplinian vent. Flow directions from the density currents suggest that the vent location is in the north-central region of the present-day lake within the Askja caldera marginal fault shown in red on Fig. 9. Descriptions of the pre-eruption depression coincide with this location.

Sharp unconformities and slump planes between the C2 and Plinian D deposits clearly suggest that ground shaking between these phases was very intense. The lower sub-unit of the Plinian deposits has the highest abundance of lithic clasts, suggesting that the initial phase of this eruption was one of opening of a new vent. Preliminary componentry data also suggest that the Plinian vent was located within the western basaltic lava-covered area. Plinian dispersal characteristics, together with the abundance of large meter-sized lithic basaltic lava and pumice bombs on the northwest side of the caldera, and meter-sized pumice bombs on the southern caldera mountains, suggest a vent location to the south and west of the inferred source of the phreatoplinian and pyroclastic surge phase (Fig. 9). The contemporary drawings of the depression and gas plumes also suggest that this vent location was in the mid-southern extent of the old caldera fault region.

Minor weaker explosive activity was synchronous with the Plinian phase, producing intensely-welded fall deposits in the southwest and northern regions of the Öskjuvatn caldera. Based on the observations described above, and the dispersal characteristics of the welded deposits (Carey et al. 2008a, b), it appears that these vents were at the peripheral extensions of two structural weaknesses, one along the southern extent of the caldera

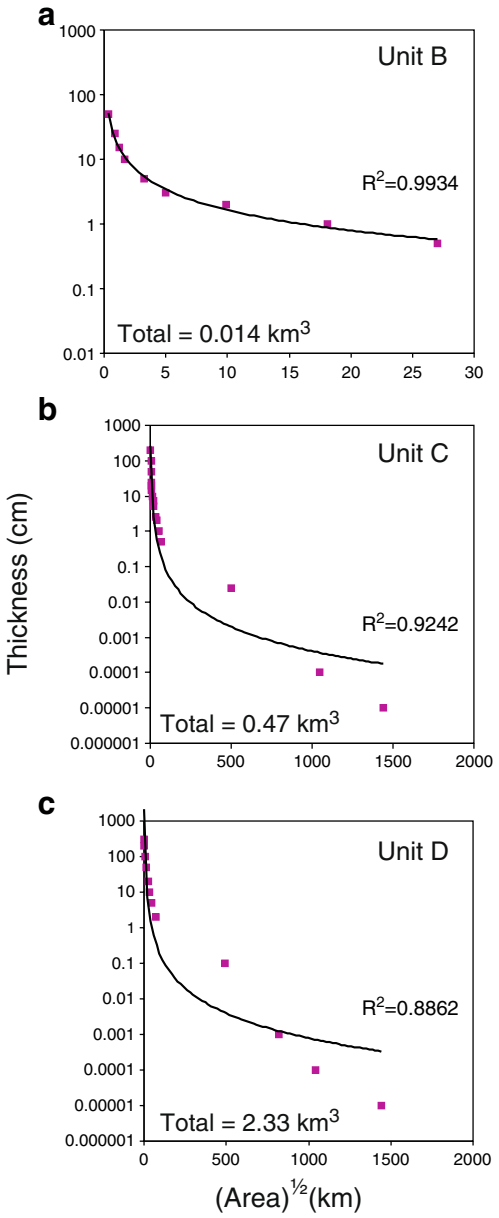

Fig. 8 Power law thinning relationships for semilog plots of thickness vs. area$^{1/2}$. This model is well-suited to unit B **a**, but fails to model accurately the medial and distal thinning trend of the unit C and D deposits **b** and **c**, even though 13 – 16 isopachs can be defined for each fall unit

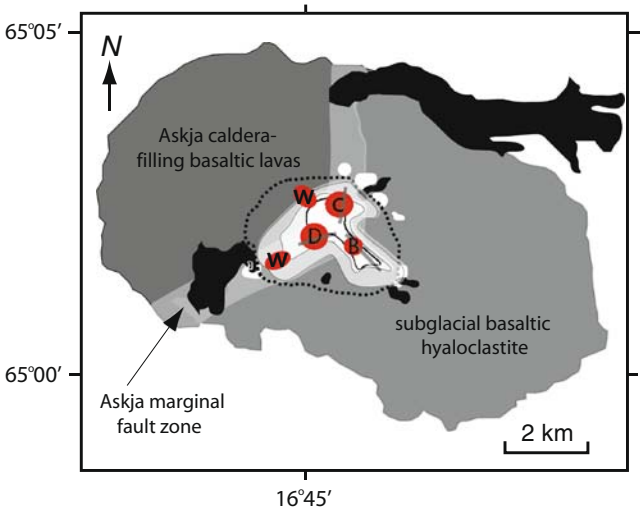

Fig. 9 Our inferred vent positions (in red) sit within the early developing shape of the Öskjuvatn caldera in 1876 (transparent white) as reconstructed by Jónsson (1942) based on descriptions made in 1876 by Johnstrup (1877). Their observations document a triangular depression, with three fracture swarms: one to the southeast, one to north and one to the west-northwest (Watts 1875; Jöhnstrup 1877, 1876). The 'small pond' of water they describe in their reports was located at the junction of these depressions. The present day form of the Öskjuvatn caldera (dashed line) was finally established in 1929. Also shown are sites of pre- and post main phase (28–29 March 1875) activity (in white and black respectively), which are focused upon the Askja marginal fault zone and the NW-SE tectonic fabric of the region

fault, and the other at the northwest extent of the NW-SE trending fault (Fig. 9).

Mass discharge rates

Durations for each of the phases are constrained approximately by historical reports (Thordarson et al. in prep); the subplinian column was observed for an hour, phreatoplinian ashfall in the medial/distal areas continued for 1 h, followed by 5–6 h of Plinian ashfall. These values permit us to calculate time-averaged mass discharge rates, which are listed in Table 3. A surprising result is the relatively low time-averaged MDR during plinian times with respect to the phreatoplinian phase. This calculation is almost an order of magnitude less than the mass discharge rate inferred from column height following the plot of Sparks (1986). We caution that the mass discharge rate calculated from the duration and estimated volume is a time-averaged value, and suggest that the peak discharge rates during the Plinian phase was of the order of 10^8 kg s^{-1}.

Comparison with other eruptions

Comparisons of dispersal with other eruptions of similar style (Fig. 10) show how each of the 1875 fall units fit into the global scale of eruption intensity. In terms of mass discharge rates, the 1875 Plinian phase is at least of comparable size to some of the better-known eruptions such as Mount St Helens 1980 (1.9×10^7 kg s^{-1}; Carey and Sigurdsson 1985) (Fig. 10; Table 3). In comparison to the other 'type' phreatoplinian eruptions from the Taupo Volcanic Zone, the Askja phreatoplinian phase appears to be a mid-intensity member of the group (10^5–10^6 kg s^{-1}; Smith 1998). The mass discharge rate of the Askja subplinian phase (2.6×10^6 kg s^{-1}) sits in the field of the 20th century eruptions of Hekla volcano (10^5 kg s^{-1} to 10^6 kg s^{-1}; Thorarinsson and Sigvaldason 1972; Gudmundsson et al. 1992; Höskuldsson et al. 2007), and also that of the May – June 1980 eruptions of Mount St Helens (~ 2 – 3×10^6 kg s^{-1}; Sarna-Wojcicki et al. 1981) (Fig. 10; Table 3).

Column height

A common method used to calculate column heights of eruptions is based on fining of clast size; the height of the eruption column can be estimated by the rate at which clast size decreases cross wind (e.g., Pyle 1989; Carey and Sparks 1986). Here we apply these methods to estimate and compare column heights for the phases of the 1875 eruption. In all three units of the main 1875 eruption, one to two segments are observed on a semilog plot of clast diameter vs. area^{½} (Fig. 11). A simple linear fit to the data is precluded by steep proximal segments for each unit, and we have used only the more distal segments for our calculations. H_b (neutral buoyancy height) can then be used to approximate H_t (total column height), by the empirical relationship H_b/H_t~0.7 (Sparks 1986). The potential of low-density pumice to be influenced by wind advection is very high, hence we use the slope of distal segments of the maximum lithic clasts. This method gives H_b and H_t values of 23 and 33 km for unit C, and 26 and 37 km for unit D, respectively (Table 4). Complexities arise when estimating column height for the distal segment of the initial subplinian phase (Fig. 11b), as calculated column heights are unreasonably low for an eruption of this volume and intensity. This is dominantly due to the lack of preserved distal primary deposits. Thus we have used the intermediate segment to apply this calculation of column height, giving H_b and H_t values of 16 and 22 km for unit B.

The method of Carey and Sparks (1986) was applied to the isopleth data for lithics found within the subplinian and Plinian fall deposits. It could not be applied to the phreatoplinian deposits due to the high degree of fragmentation of the lithic components, which are uniformly fine ash. Column heights for the subplinian and Plinian phases calculated using this method are 8 km and 26 km respectively (Table 4).

Table 3 Table of eruption parameters for the 1875 units, and other subplinian, phreatoplinian and Plinian eruptions listed in the literature (see footnote). Mass discharge rate (MDR) and volumetric discharge rate (VDR) were calculated for the 1875 units using historical records of duration and DRE values. Bulk density measurements down the dispersal axis for each fall unit, were used to calculate DRE values. Clast half distance (b_c) is defined as the radial distance over which the maximum clast diameter decreases by half (Pyle 1989). Thinning half distance (b_t) is the distance over which the deposit thins by half

	Deposit	Column height (km)	MDR (kg s^{-1})	VDR (m^3 s^{-1})	DRE (km^3)	volume (km^3)	Time (hours)	Total mass (kg)	*Bc* (km)	Bt (km)
	Subplinian									
1	Vesuvius subplinian 1631	17-21	3 - 6 x 10^7			0.07	11			2.3
2	Furnas 1630 L2	12.5	4 - 6 X 10^6		0.0208	0.067	2.8	49.9 X 10^9		
2	Furnas 1630 L3	13.5	5 - 8 X 10^6		0.0327	0.076	3.1	78.4 X 10^9		
3	Hekla 1970	16							2	2
4	Hekla 1991	11.5				0.02	3			
5	Hekla 2000	12.8		2.6 x 10^3		0.0001	0.5			
6	MSH May 25 1980	15			0.007	0.016		0.42 x 10^{11}	3.4	2.6
									3.4	14.8
7	MSH June 12 1980	14	2.7 x 10^6		0.0078	0.017	4.5	0.45 x 10^{11}		
	Askja 1875 Unit B	**8 (a)**	**2.6 x 10^6**	**3.9 x 10^3**	**0.004**	**0.014**	**1**	**9.4 x 10^9**		**0.32**
										1.1
	Phreatoplinian eruptions									
8	Rotongaio ash (Taupo 181 AD)		10^5 - 10^7		0.8	2.1	days to months			2.9-4.9
8	Hatepe Ash (Taupo 181 AD)		10^7 - 10^8		0.7	1.8	days to months			4.4-8.6
9	Oruanui (Taupo 26 ka)						weeks to months			12.6-110
10	Hakone, Japan 13000 BP					16		1.1 x 10^{13}		1.5-3.3
	Askja 1875 Unit C	**22.8 (b)**	**6.8 x 10^7**	**1.2 x 10^5**	**0.104**	**0.45**	**1**	**4.8 x 10^{11}**		**0.4**
										6.7
										7.4
										44.4
										67.4
	Plinian eruptions									
11	Vesuvius 79 AD (grey)	32	1.5 x 10^8		2.1		9.5	6.1 x 10^{12}	4.2	7.6
12	Huaynaputina 1600 stage 1	34-46	2.8 x 10^8		8.8		20	2.1 x 10^{13}	8.34 (MP)	1
									3.97 (ML)	6.5
										50.5
13	Novarupta 1912 episode 1	23-26	0.7 -1.0 x 10^8		2.1	8.8	60	4.8 10^{12}		
13	novarupta 1912 episode 2	22-25	0.6 - 2 x 10^8		1.99	4.8	combined	4.8 x 10^{12}		22
13	Novarupta 1912 episode 3	17-23	0.2 - 0.4 x 10^8		1.66	3.4	hours	4.0 x 10^{12}		18.8
14	Quizapu 1932	25-32	1.5 x 10^8	6.2 x 10^4	4.05	9.5	18-25			1.3
										5.4
										62.4
15	Mt St Helens May 18 1980	19	1.9 x 10^7		1.1	0.24	9.1	6.3 x 10^{11}	3.3	2.8
									3.3	34.4
16	Hudson 1991									3.1
										8.5
										62.5
	Askja Unit D	**26 (a)**	**2.5 x 10^7**	**6.9 x 10^4**	**0.213**	**1.37**	**6**	**5. x 10^{11}**		**1.1**
			3.5 x 10^7 (peak)	**9.5 x 10 4 (peak)**			**4**			**5.3**
										37.2
										67.4

References for data: 1. Rosi et al., (1993); 2. Cole et al., (1995); 3. Thorarinsson (1972); 4. Gudmundsson et al., (1992); 5. Hoskuldsson et al., (2007); 6. Sarna-Wojcicki et al., (1981); 7. Sarna-Wojcicki et al., (1981); 8. Smith (1998); 9. Wilson (2001); 10. Hayakawa et al., (1990); 11. Carey and Sigurdsson (1985), Sigurdsson and Carey (1985); 12. Adams et al., (2001); 13. Fierstein and Hildreth (1992); 14. Hildreth and Drake (1992); 15. Sarna-Wojcicki et al., (1981); 16. Scasso et al., (1994). Column heights calculated for the Askja deposits; (a) Carey and Sparks (1986); (b) Pyle (1989).

We feel that the methods of Pyle (1989) and Carey and Sparks (1986) give the most reasonable estimations of column heights, i.e., the subplinian plume rising to 8 km, and Plinian plume to 26 km (Tables 3, 4). Historical accounts converge on column heights of 27 – 30 km for the phreatoplinian and Plinian columns (Thoroddsen 1913, 1925; Thordarson et al. in prep).

Discussion

Calculating tephra-fall volumes based on power-law and exponential thinning

The subplinian B phase of the eruption produced a deposit for which nine isopachs could be constrained, and power-law and exponential thinning methods give similar calculated volumes (Table 1a). Similar to the Ruapehu 1996 subplinian deposit described by Bonadonna and Houghton (2005), the high resolution of the power-law trend, constrained by the large number of tightly-spaced isopachs together with the rapidly thinning nature of the deposit, leads to the power-law method being a valid technique to calculate volume.

The more widespread deposits from the Plinian and phreatoplinian phases also yield large datasets (13 and 16 isopachs, respectively). Close to source the deposits are moderately-well described by a power-law trend that fails, however, to constrain the distal data (Figs. 8b, c). The entire datasets can only be modeled adequately by a segmented exponential thinning trend with four to five segments (Figs. 7b, c). The problem for both datasets lies in the distal field.

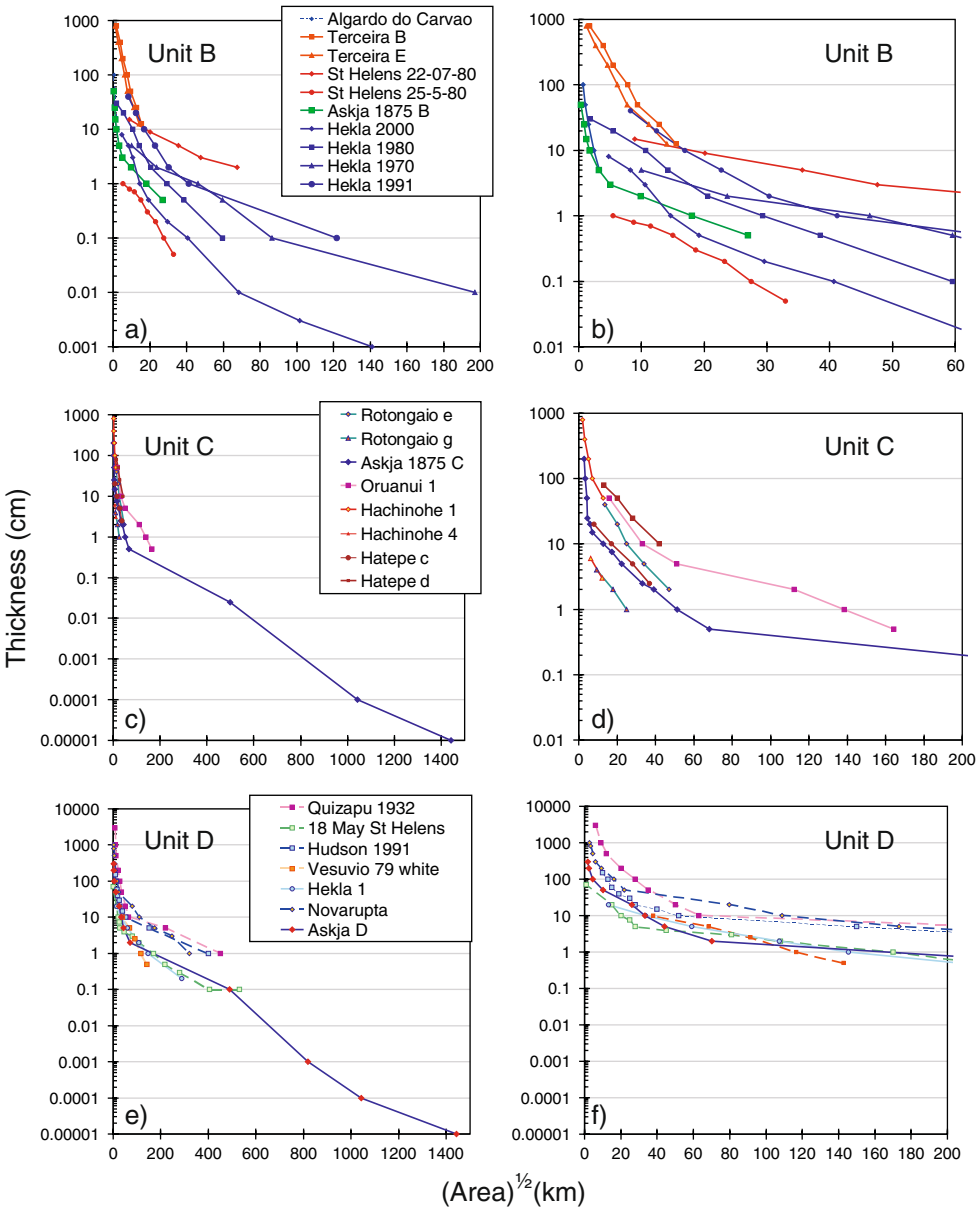

Fig. 10 Semilog plots of thickness vs. area$^{1/2}$ for each of the fall units, together with the dispersal trends for other eruptions of similar type. **b**, **d** and **f** are expanded proximal equivalents to emphasize the proximal thinning trends in each case

There are significant challenges in accurately using field data in thinning models to calculate volumes. In terms of the collection of data, it is important not only to constrain many isopachs, but also to have consistent intervals of isopach contours. An irregularity of contour spacing may lead to apparent deviation in thinning trend, in particular when using a power-law model. The diversity of processes operating in volcanic plumes also presents a challenge for deposit thinning models. The process of particle aggregation, which occurs very commonly in plumes, can shift a power-law trend of thinning based on the particle Reynolds number described in numerical models, to a segmented exponential thinning trend (Bonadonna and Phillips, 2003) (e.g., 1980 Mount St Helens and 1932 Quizapu eruptions; Sorem 1982; Carey and Sigurdsson 1982; Dartayet 1932; Lunkenheimer 1932). In addition, plume margin instabilities, which are also common features of both dry, and particularly wet eruptions, may lead to the production of co-Plinian pyroclastic density currents (e.g. Hatepe Plinian phase, Taupo 181 AD, Talbot et al. 1994; Vulcan, Rabaul, 1937, see reference in McKee et al. 1985; and Ukinrek Maars, Alaska 1977, Self et al. 1980), and the net effect is an apparent over-thickening of the proximal deposits.

Secondary pyroclast transport after deposition is a natural process; however, timescales are typically accelerated due to the alpine and harsh weather environments surrounding volcanoes such as Askja. Recent eruptions (<100 years) where the deposits are well preserved, deposited predominantly on land, and/or documented immediately, are more likely to follow the idealized power-law thinning trend defined by numerical models (e.g., Ruapehu volcano, New Zealand; Bonadonna and

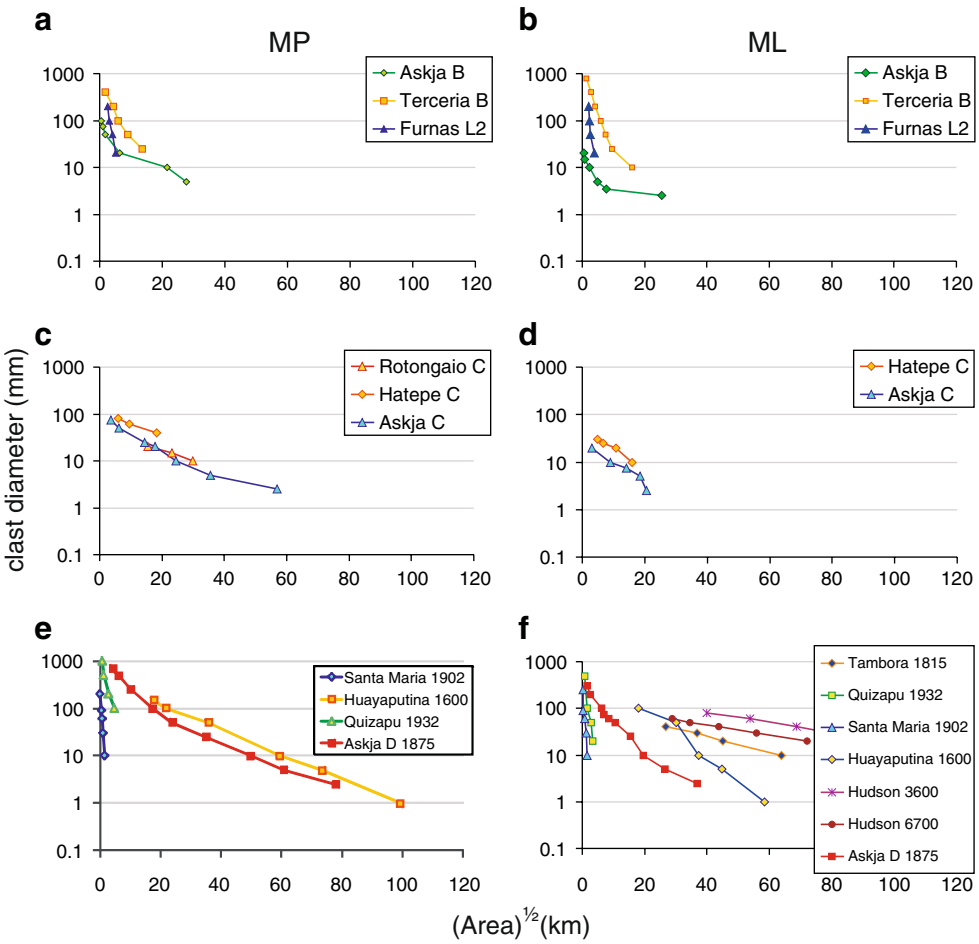

Fig. 11 Semilog plots of clast diameter vs. area$^{1/2}$ displaying the maximum pumice (MP) and maximum lithic (ML) data for each 1875 unit in comparison to other eruptions. All of the Askja fall units plot in the lowermost portion of their respective fields. However, only limited datasets were available for other eruptions. Using the method described in Pyle (1989), column heights were estimated using the ML plot

Houghton 2005). However, pre-historic eruptions (including Askja 1875) are likely to be eroded and/or reworked and thus may be more suited to the application of a segmented exponential thinning method (e.g. Novarupta 1912, Houghton et al. 2004).

The problem of incomplete data sets

The Askja 1875 fall units have well-constrained proximal and far-distal thickness measurements and are thus particularly well-suited for comparison of volume calculations involving missing distal or proximal data, which is often the case for high intensity caldera-forming eruptions. In the following examples we simulate two separate scenarios; first, a situation analogous to the deposits of the Taupo 181 AD eruption, where Plinian and phreatoplinian deposits are not exposed at distances less than 4 km from the inferred vent locations and thus no proximal data are available. Secondly, we simulate a theoretical case, in which there is no exposure of the 1875 deposits outside of Iceland (i.e. greater than 150 km from Askja caldera). For the subplinian scenario, we consider an option where no deposits are observed at distances greater than 15 km from vent, which is often the case for historic subplinian falls at Etna volcano (e.g., Branca and del Carlo 2005).

Exponential thinning models applied to the 1875 units without proximal data<4 km from vent produced volumes that were 99%, 87% and 105% of the actual volumes for the subplinian, phreatoplinian and Plinian units respectively (Figs. 12a, b, c; Table 5). There was also an expected reduction in the number of required exponential line segments for unit C from five to four. A power-law fit to

Table 4 Estimated column heights (in kilometers) for each of the 1875 fall units using the methods of Pyle (1989) and Carey and Sparks (1986)

Unit	Pyle (1989)		Carey and Sparks (1986)	
km				
	Hb	*Ht*	*Hb*	*Ht*
1875 B	16	22	8	10
1875 C	23	23	—	—
1875 D	26	26	26	34

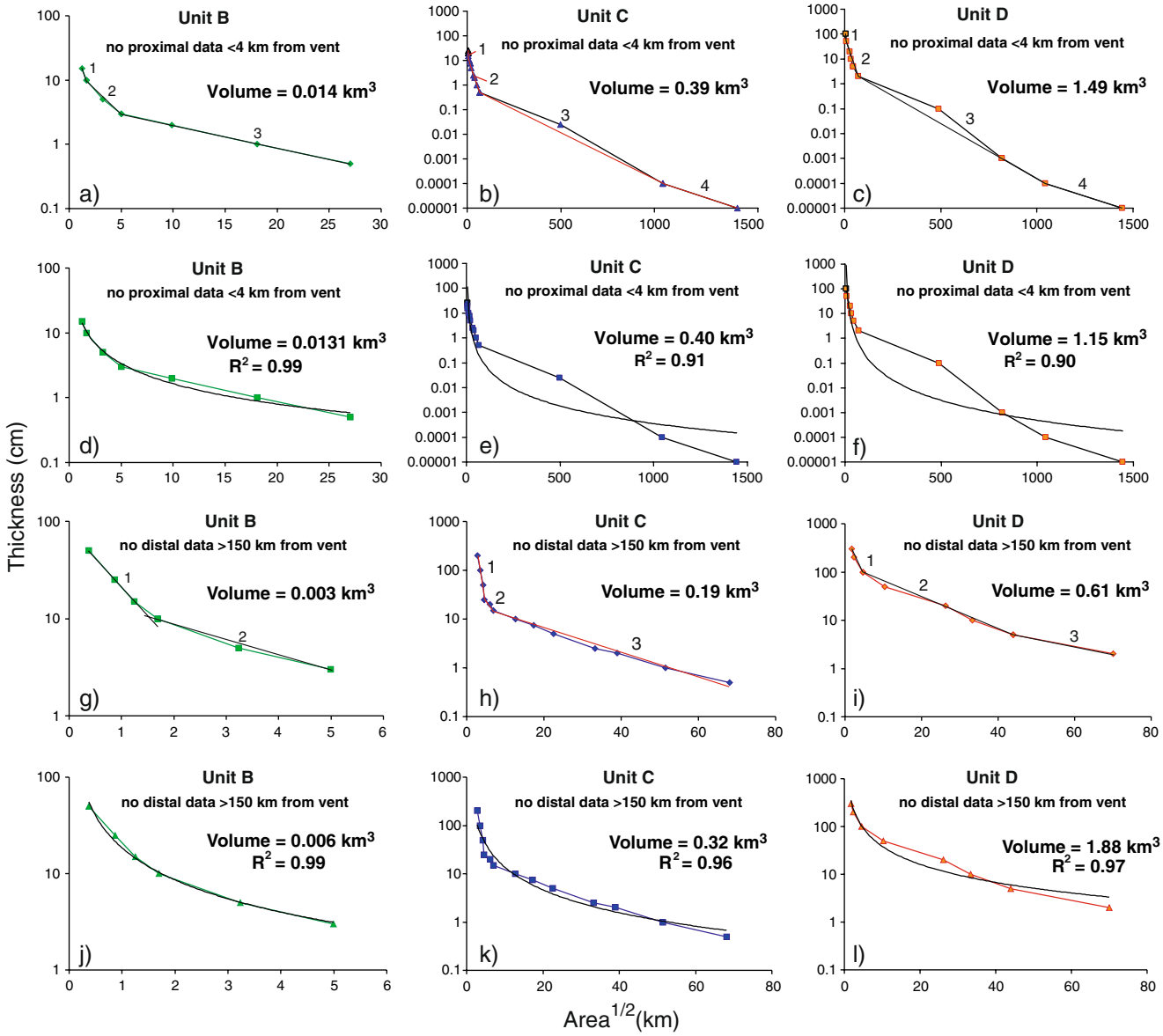

Fig. 12 Semilog plots of thickness vs. area shown for the 1875 fall units. For unit B, there are two different scenarios: **a** and **d** no proximal data <4 km from vent; **g** and **j** no distal data>15 km from vent. Both segmented exponential **a** ang **d** and power-law thinning models **d** and **j** are shown for comparison. Both models were unable to calculate accurate volumes when distal data were missing, resulting in very inaccurate calculations in **g** and **j**. When proximal data were missing, both models calculated fairly accurate volumes, shown in **a** and **d** Semilog plots of thickness vs. area$^{1/2}$ shown for the Unit C deposit, for two different scenarios: **b** and **e** no proximal data <4 km from vent; **h** and **k** no distal data>150 km from vent. Both methods could not approximate the volume well where distal data is not available. However, the power-law method **k** was more accurate than the exponential method **h**. In absence of proximal data, both methods resulted in similar values and slightly underestimate the true volume **b** and **e**. Semilog plots of thickness vs. area$^{1/2}$ shown for the Unit D deposit, in two different scenarios: **c** and **f** no proximal data <4 km from vent; (i) and (l) no distal data>150 km from vent. Without distal data, the power-law method overestimates the volume, however the segmented exponential method severely underestimates the volume. Without proximal data, the power-law method underestimates the volume, and the segmented exponential thinning model slightly overestimates the volume

the same data set produced volumes that were 92%, 89% and 84% of the actual volumes, respectively (Figs. 12d, e, f; Table 5). Without the distal data sets, segmented exponential thinning produced volumes that were 21%, 42% and 45% of the actual volumes for the subplinian, phreatoplinian and Plinian units respectively, and a reduction of segments by one for each unit (Figs. 12g, h, i; Table 5). A power-law fit without the distal data produced volumes that were 42%, 72% and 129% of the actual volumes respectively (Figs. 12j, k, L; Table 5).

Table 5 Volumes using the segmented exponential thinning model for each of the 1875 fall units, and comparisons to calculated volumes when proximal and distal data are missing using both power-law and segmented exponential thinning models. When the exponential thinning model is used on incomplete datasets, the number of recognized segments (listed in right column) is typically reduced

Unit	Volume (km^3)	% of actual volume	No. segments
Exponential model without proximal data			
Unit B	0.0142	99.3	3
Unit C	0.39	86.7	4
Unit D	1.49	105.0	4
Power law model without proximal data			
Unit B	0.0131	91.7	
Unit C	0.40	89.3	
Unit D	1.15	83.8	
Exponential model without distal data			
Unit B	0.0030	21.0	2
Unit C	0.19	42.4	3
Unit D	0.61	44.5	3
Power-law model without distal data			
Unit B	0.0060	42.0	
Unit C	0.32	72.1	
Unit D	1.88	128.5	
Actual volumes			
Unit B	0.0143	100.0	3
Unit C	0.45	100.0	5
Unit D	1.37	100.0	4

Summary

In summary, both the segmented exponential thinning and power-law methods generally underestimated the volume of the deposits when either proximal or distal data were not available. Both methods are only slightly sensitive to a lack of proximal exposure, but loss of distal data has a drastic effect on volume calculations.

When proximal data (< 4 km) were missing, both techniques calculated the volume to within 17 % of the full calculated value. The exponential thinning model provided fairly good approximations of the true volume except for the Askja C phreatoplinian phase, because it is significantly over-thickened, with ~16 % of the volume in the first segment (< 4 km). For units B and D, missing proximal data had a minor effect (+/− 5 %). Using the power-law model, the loss of proximal data for each of the units reduced the value of maximum thickness (T_o), and the R^2 fit, leading to an underestimation of the volume. When proximal data are missing, the choice of power-law or exponential thinning models must be evaluated based on the remaining more distal data (i.e., scale of caldera collapse). It appears that a segmented exponential thinning model would be best if a) only few data are missing and b) no proximal over-thickening is suspected.

When distal data were missing, the degree of underestimation using the segmented exponential method was a function of the volume represented by the last segments. For example, losing the last two distal segments for unit C and final segment of unit D represents thicknesses of <0.5 and <2 cm of tephra, respectively, which are large components of the total volume. Similarly with unit B, the most distal segment is<3 cm thick. If minimal distal ash is lost (e.g., 18 May 1980 Mount St. Helens fall), exponential thinning is a good approximation. The power-law method is always difficult to apply when distal data are missing. This is predominantly due to the difficulty in extrapolating the thinning trend into the distal field and the fact that the volume calculation is very susceptible to the integration limits of *C* (observed distance of plume spreading). For reasonable limits of *C*, based on the artificially-constrained data (i.e., without distal data), the power-law method both greatly underestimated volumes for units B and C and greatly overestimated the volume for unit D (Table 5).

This dataset broadly supports the studies conducted by Bonadonna and Houghton (2005) where a power-law thinning model is considered to be better suited to deposits for which distal data are missing, especially if it is possible to constrain the limit of downwind spreading of the umbrella cloud via satellite imagery. This method could also be applied in a setting where the size and/or intensity of the eruption can be estimated, to interpolate the thinning trend into the distal field and thus calculate an approximate volume. However, there are some caveats to using the power-law method to estimate volume when data are missing. First, if the intermediate data points cannot adequately define the zone of curvature for the power-law fit (as also shown in Bonadonna et al. 1998), then this method would be extremely unreliable. Second, if the eruption is prehistoric, then the choice of the maximum integration limit (*C*) will be problematic. However, ash shards in drill core, such as the 1875 ash found throughout Scandinavia and northern Germany, may define the integration limit (*C*), enhancing the reliability of the power-law method.

Conclusions

Our study focusing on the dispersal characteristics of the main phases of the 1875 eruption of Askja volcano, together with detailed historical observations, has implications for eruption dynamics. The combination of very proximal and very far-distal data for this eruption has supplied a detailed dataset which enabled us to test the validity of the segmented

exponential thinning model and power law thinning model for each of the 1875 fall units. We have been able to make calculations of eruptive volumes and evaluate the bias of the volume data when proximal or distal data are missing. Proximal exposures within 1 km from inferred vents have permitted us to examine dispersal characteristics of the deposits, volume calculations and locations of vents active during each phase. However, caldera collapse following large Plinian eruptions is very common and removes very proximal deposits, which hold important keys to eruption and plume dynamics. A further~500 radial meters of caldera widening would have destroyed the proximal exposures at Askja, leading to difficulty documenting proximal thinning behavior and inaccurate positioning of the active vents.

References

Adams NK, Da Silva SL, Self S, Salas G, Schubring S, Permenter JL, Arbesman K (2001) The physical volcanology of the 1600 eruption of Huaynaputina, southern Peru. Bull Volcanol 62:493–518

Bonadonna C, Ernst GGJ, Sparks RSJ (1998) Thickness variations and volume estimates of tephra fall deposits: the importance of particle Reynolds number. J Volcanol Geotherm Res 81:173–187

Bonadonna C, Phillips J (2003) Sedimentation from strong volcanic plumes. J Geophys Res 108:2340–2368

Bonadonna C, Houghton BF (2005) Total grain-size distribution and volume of tephra fall deposits. Bull Volcanol 67:441–456

Boygle JE (2004) Towards a Holocene tephrachronology for Sweden: geochemistry and correlation with the North Atlantic tephra stratigraphy. J Quat Sci 19:103–109

Branca S, Del Carlo P (2005) Types of eruptions of Etna volcano AD 1670–2003: Implications for short-term behavior. Bull Volcanol 67:732–742

Brandsdottir B (1992) Historical accounts of earthquakes associated with eruptive activity in the Askja volcanic system. Jökull 42:1–12

Carey RJ, Houghton BF, Thordarson TT (2008a) Complex welding of proximal Plinian deposits I: Regional welding. (in press). J Volcanol Geotherm Res 171:1–19

Carey RJ, Houghton BF, Thordarson TT (2008b) Complex welding of proximal Plinian deposits II: Local welding. (in press). J Volcanol Geotherm Res 171:20–44

Carey SN, Sigurdsson H (1982) Influence of particle aggregation on deposition of distal tephra from the May 18, 1980, eruption of Mount St Helens volcano. J Geophys Res 87:7061–7072

Carey SN, Sigurdsson H (1985) The May 18, 1980 eruption of Mount St-Helens.2. Modeling of dynamics of the Plinian phase. J Geophys Res 90:2948–2958

Carey SN, Sparks RSJ (1986) Quantitative models of fallout and dispersal of tephra from volcanic eruption columns. Bull Volcanol 48:109–125

Carey S, Sigurdsson H (1987) Temporal variations in column height and magma discharge rate during the 79 A.D. eruption of Vesuvius. Geol Soc Am Bull 99:303–314

Cole PD, Queiroz G, Wallenstein N, Gaspar JL, Duncan AM, Guest JE (1995) An historic subplinian/phreatomagmatic eruption; the 1630 AD eruption of Furnas volcano, Sao Miguel, Azores. J Volcanol Geotherm Res 69:117–135

Dartayet M (1932) Observacíon de la lluvia de cenizas del 11 de abril de 1932 en LaPlata. Rev Astron (Buenos Aires) 4:183–187

Fierstein J, Hildreth W (1992) The Plinian eruptions of 1912 at Novarupta, Katmai National Park, Alaska. Bull Volcanol 54:646–684

Fierstein J, Nathenson M (1992) Another look at the calculation of fallout tephra volumes. Bull Volcanol 54:156–167

Gudmundsson A, Oskarsson N, Gronvold K, Saemundsson K, Sigurdsson O, Stefansson R, Gislason SR, Einarsson P, Brandsdottir B, Larsen G, Johannesson H, Thordarson T (1992) Hekla 1991 eruption. Bull Volcanol 54:238–246

Hayakawa Y (1990) Mode of eruption and deposition of the Hachinohe phreatoplinian Ash from the Towada Volcano, Japan. Geogr Rep Tokyo Metropolitan Univ 25:167–182

Hildreth W, Drake RE (1992) Volcano Quizapu, Chilean Andes. Bull Volcanol 54:93–125

Höskuldsson Á, Óskarsson N, Pederson R, Grönvold K, Vogfjörð K, Ólafsdóttir R (2007) The millennium eruption of Hekla in February 2000. Bull Volcanol 70:169–182

Houghton BF, Wilson CJN, Fierstein J, Hildreth W (2004) Complex proximal deposition during the Plinian eruptions of 1912 at Novarupta, Alaska. Bull Volcanol 66:95–133

Inman DL (1952) Measures for describing the size distribution of sediments. J Sed Petrol 22:125–145

Jöhnstrup F (1876). Det danske geografiske Selskabs Tidsskrift 1ste Bind Side 58– 59

Jöhnstrup F (1877). Indberetning om den af Professor Johnstrup foretagne Undersögelsesreise paa Island i Sommerem 1876 (hermed 2 kort og 2 tegninger), Særskilt? Aftryk af Rigsdag-stidenden for den 29de ordentlig Samling 1876–77, Tillæg B. J. H. Schultz, Köbenhavn, Sp. 899–926

Lunkenheimer F (1932) La erupción del Quizapu en abril de 1932. Rev Astron (Buenos Aires) 4:173–182

Manville V, Hodgson KA, Houghton BF, Keys JR, White JDL (2000) Tephra, snow and water: complex sedimentary responses at an active snow-capped stratovolcano, Ruapehu, New Zealand. Bull Volcanol 62:278–293

McKee C, Johnson RW, Lowenstein PL, Riley SJ, Blong RJ, Ours DeSaint, Talai B (1985) Rabaul caldera, Papua New Guinea: volcanic hazards, surveillance, and eruption contingency planning. J Volcanol Geotherm Res 23:195–237

Mohn H (1878) Askeregnen den 29de-30-te Marts 1875. Forhandlinger I Videnskapsselskabet I Christiania aar 1877 10:89–92

Nordenskiöld AE (1876) Report on Askja ash fall. Aftonbladet, 1st April,1876

Oldfield F, Thompson R, Crooks PRJ, Gedye SJ, Hall VA, Harkness DD, Housley RA, McCormac FG, Newton AJ, Pilcher JR, Renberg I, Richardson N (1997) Radiocarbon dating of a recent high-lattitude peat profile: Stor Amyran, northern Sweden. The Holocene 7:282–290

Persson C (1971) Tephrachronological investigation of peat deposits in Scandinavia and on the Faeroe Islands. Sveriges Geologiska Undersoknin 65:1–34

Pilcher J, Bradley A, Raymond S, Francus P, Anderson S, Lesleigh (2005) A Holocene tephra record from the Lofoten Islands, Arctic Norway. Boreas 34:136–156

Pyle DM (1989) The thickness, volume and grain-size of tephra fall deposits. Bull Volcanol 51:1–15

Pyle DM (1990) New estimates for the volume of the Minoan eruption. Thera and the Aegean World. D. A. Hardy. London, The Thera Foundation. III:113–121

Rosi M, Principe C, Vecci R (1993) The 1631 Vesuvius eruption A reconstruction based on historical and stratigraphical data. J Volcanol Geotherm Res 58:151–182

Sarna-Wojcicki AM, Shipley S, Waitt RB, Dzurisin D, Wood SH (1981) Areal distribution, thickness, mass, volume and grain size of air-fall ash from the six major eruptions of 1980. In: Lipman PW, Mullineaux DR (eds) The 1980 eruptions of Mount St. Helens, Washington. US Geol Surv Prof Pap 1250:577–628

Scasso RA, Corbella H, Tiberi P (1994) Sedimentological analysis of the tephra from the 12–15 August 1991 eruption of Hudson volcano. Bull Volcanol 56:121–132

Self S, Kienle J, Huot JP (1980) Ukinrek Maars, Alaska, II. Deposits and formation of the 1977 craters. J Volcanol Geotherm Res 7:39–65

Self S, Sparks RSJ (1978) Characteristics of widespread pyroclastic deposits formed by the interaction of silicic magma and water. Bull Volcanol 41:196–212

Sigurdsson H, Sparks RSJ (1978a) Lateral magma flow within rifted Icelandic crust. Nature. 274:126–130

Sigurdsson H, Sparks RSJ (1978b) Rifting episode in north Iceland in 1874–1875 and the eruptions of Askja and Sveinagja. Bull Volcanol 41:1–19

Sigurdsson H, Carey SN, Cornell W, Pescatore T (1985) The eruption of Vesuvius in A.D. 79. Nat Geog Res Explor 1:332–387

Sigvaldason GE (1979) Rifting, magmatic activity, and interaction between acid and basic liquids: The 1875 Askja eruption in Iceland. Report 7903, Nordic Volcanological Institute, Reykjavik, Iceland

Sigvaldason GE (2002) Volcanic and tectonic processes coinciding with glaciation and crustal rebound: an early Holocene rhyolitic eruption in the Dyngjufjoll volcanic centre and the formation of the Askja caldera, north Iceland. Bull Volcanol 64:192–205

Smith RT, Houghton BF (1995a) Delayed deposition of plinian pumice during phreatoplinian volcanism: the 1800-yr-B.P. Taupo eruption, New Zealand. J Volcanol Geotherm Res 67:221–226

Smith RT, Houghton BF (1995b) Vent migration and changing eruptive style during the 1800a Taupo eruption: new evidence from the Hatepe and Rotongaio phreatoplinian ashes. Bull Volcanol 57:432–439

Smith RT (1998) Models for Units 3 and 4 of the Taupo eruption. PhD thesis, University of Canterbury, Canterbury, New Zealand.

Sorem RK (1982) Volcanic ash clusters: tephra rafts and scavengers. J Volcanol Geotherm Res 13:63–71

Sparks RSJ, Wilson L, Sigurdsson H (1981) The pyroclastic deposits of the 1875 eruption of Askja, Iceland. Phil Trans Royal Soc Lond 299:241–273

Sparks RSJ (1986) The dimensions and dynamics of volcanic eruption columns. Bull Volcanol 48:3–15

Talbot JP, Self S, Wilson CJN (1994) Dilute gravity current and rain-flushed ash deposits in the 1.8 ka Hatepe Plinian deposit, Taupo, New Zealand. Bull Volcanol 56:538–551

Thorarinsson S, Sigvaldason GE (1972) The Hekla eruption of 1970. Bull Volcanol 36:269–288

Thordarson T, Carey RJ, Houghton BF (in prep) Historical accounts of 19th and 20th century volcanic eruptions at the Askja volcano (Iceland) with a special reference to the 1874-1876 volcano-tectonic event

Thoroddsen T (1913) Ferðabók I, pp 255–380

Thoroddsen T (1925) Die Geschichte der Islandischen Vulkane. A. F. Host and Son Konglige Hof-Boghandle, Copenhagen, 458 pp

van den Bogaard C, Schmincke HU (2002) Linking the North Atlantic to central Europe: a high-resolution Holocene tephrochronological record from Northern Germany. J Quat Sci 17:3–20

Watt SFL, Pyle DM, Mather TA, Martin RS, Mattews NE (2009) Fallout and distribution of volcanic ash over Argentina following the May 2008 explosive eruption of Chaitén. Chile. J Geophys Res 114:B04207. doi:10.1029/2008JB006219

Watts WL (1875) Bréf frá herra W. L. Watts (Letter from Mr W. L. Watts). Þjóðólfur, 27:109

Watts WE (1876) Across Vatnajökull. Longmans and Co, London, 106 pp